

# Inhibition of Tau Filament Formation by Conformational Modulation

Elias Akoury,<sup>†</sup> Michal Gajda,<sup>†</sup> Marcus Pickhardt,<sup>‡</sup> Jacek Biernat,<sup>‡</sup> Pornsuwan Soraya,<sup>||</sup> Christian Griesinger,<sup>†</sup> Eckhard Mandelkow,<sup>\*,‡,§,#</sup> and Markus Zweckstetter<sup>\*,†,⊥,#</sup>

<sup>†</sup>Department for NMR-based Structural Biology, Max Planck Institute for Biophysical Chemistry, 37077 Göttingen, Germany

<sup>‡</sup>German Center for Neurodegenerative Diseases (DZNE), Ludwig–Erhard–Allee 2, 53175 Bonn, Germany

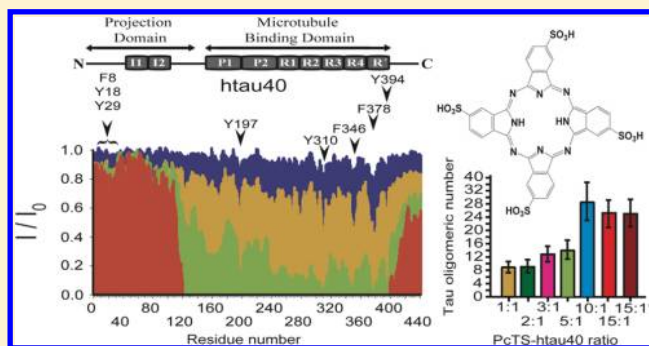
<sup>§</sup>CAESAR Research Center, Ludwig–Erhard–Allee 2, 53175 Bonn, Germany

<sup>||</sup>RG Electron Spin Resonance Spectroscopy, Max Planck Institute for Biophysical Chemistry, Am Fassberg 11, 37077 Göttingen, Germany

<sup>⊥</sup>German Center for Neurodegenerative Diseases (DZNE), Göttingen, Germany

## S Supporting Information

**ABSTRACT:** Antiaggregation drugs play an important role in therapeutic approaches for Alzheimer's disease. Although a large number of small molecules that inhibit the aggregation of the tau protein have been identified, little is known about their mode of action. Here, we reveal the mechanism and the nature of tau species that are generated by interaction of tau with the organic compound phthalocyanine tetrasulfonate (PcTS). We demonstrate that PcTS interferes with tau filament formation by targeting the protein into soluble oligomers. A combination of NMR spectroscopy, electron paramagnetic resonance, and small-angle X-ray scattering reveals that the soluble tau oligomers contain a dynamic, noncooperatively stabilized core with a diameter of 30–40 nm that is distinct from the core of tau filaments. Our results suggest that specific modulation of the conformation of tau is a viable strategy for reduction of pathogenic tau deposits.



## INTRODUCTION

Neurodegenerative diseases share related pathological processes characterized by the generation of proteinaceous deposits exhibiting excessive  $\beta$ -sheet structures.<sup>1</sup> Growing evidence has implicated the aggregates in the onset, progression, and clinical symptoms of these disorders.<sup>2</sup> The most widespread dementia syndrome is Alzheimer's Disease (AD), which is characterized by the progressive accumulation of extracellular senile plaques consisting of  $\beta$ -amyloid polypeptide and intracellular neurofibrillary tangles consisting of tau protein.<sup>3,4</sup>

Tau protein belongs to the class of "natively unfolded" or intrinsically disordered proteins.<sup>5,6</sup> It is abundant in neuronal axons and interacts with tubulin to stabilize and promote microtubule assembly for the transport of vesicles and organelles.<sup>7</sup> In solution, tau is highly dynamic with an intricate domain structure.<sup>8</sup> During the course of AD progression, tau becomes excessively phosphorylated, loses its function, and aggregates into neurofibrillary tangles.<sup>4</sup> The accumulation of tau aggregates is a multistep process that involves the formation of various transient species. Increasing evidence suggests that small oligomeric species contribute to tau-mediated neurotoxicity.<sup>9</sup>

So far, only symptomatic treatment is available for AD and other protein misfolding diseases, and new therapeutic concepts range from tau vaccinations<sup>10</sup> and antiphosphorylation

strategies<sup>11</sup> to microtubule-stabilizing<sup>12</sup> and antiaggregation drugs.<sup>13–22</sup> One important class of aggregation inhibitors are porphyrins such as phthalocyanine tetrasulfonate (PcTS).<sup>16,22,23</sup> PcTS has been widely investigated for its in vivo prophylactic and therapeutic effects in scrapie disease and inhibits the formation of protease-resistant prion protein aggregates.<sup>23,24</sup> In addition, PcTS can interfere with tau aggregation and is able to disassemble tau filaments.<sup>16</sup> By taking advantage of its chelating and molecular self-assembly properties, PcTS was also employed to remove the redox-active metals that induce toxic  $A\beta_{40}$  oligomeric species and to convert the aggregates into an amyloid fibrillar meshwork.<sup>25</sup>

Despite the wealth of potential inhibitors of tau aggregation, little is known about the mechanisms of inhibition and the nature of the generated tau species. Here, we study the interaction of PcTS with 441 residue human tau protein (Figure S1, Supporting Information). Using a combination of NMR spectroscopy, electron paramagnetic resonance (EPR), and small-angle X-ray scattering (SAXS), we reveal detailed insights into the mechanisms of tau aggregation inhibition and the structure and dynamics of soluble tau oligomers.

Received: January 1, 2013

Published: January 29, 2013

## EXPERIMENTAL SECTION

**Proteins and Reagents.** Unlabeled and labeled wild-type and mutated human tau protein isoforms and constructs (htau40, htau24, htau23, K18) were expressed and purified as described previously.<sup>26</sup> Briefly, proteins were expressed in the vector pNG2 (a derivative of pET-3a; Merck) in *Escherichia coli* strain BL21(DE3). The expressed proteins were purified from bacterial extracts by making use of the heat stability of the protein and by fast protein liquid chromatography (FPLC) with a SP-Sepharose column (GE Healthcare). To label uniformly the tau proteins with <sup>15</sup>N and <sup>13</sup>C isotopes, *E. coli* bacteria were grown in minimal medium containing 1 g/L <sup>15</sup>NH<sub>4</sub>Cl and 4 g/L D-Glucose (<sup>13</sup>C-6), or 1 g/L <sup>15</sup>NH<sub>4</sub>Cl alone. The cell pellets were resuspended in extraction buffer (50 mM MES, 500 mM NaCl, 1 mM MgCl<sub>2</sub>, 1 mM EGTA, 5 mM DTT, pH 6.8) complemented with protease inhibitor mix, disrupted with a French press, and boiled for 20 min. The soluble extract was isolated by centrifugation, and the supernatant was dialyzed against buffer A (20 mM MES, 50 mM NaCl, 1 mM EGTA, 1 mM MgCl<sub>2</sub>, 2 mM DTT, 0.1 mM PMSF, pH 6.8) and loaded on an FPLC SP-Sepharose column. The proteins were eluted by a gel-filtration column by a linear gradient of buffer B (20 mM MES, 1 M NaCl, 1 mM EGTA, 1 mM MgCl<sub>2</sub>, 2 mM DTT, 0.1 mM PMSF, pH 6.8). The tau isoforms were separated from breakdown products by a gel-filtration column Superdex G-200 (GE Healthcare).

PcTS was purchased from MP Biomedicals (MP Biomedicals S.A. Heidelberg, Germany). ThS, urea, and GuSCN were purchased from Sigma (Sigma-Aldrich Chemie GmbH, Schnelldorf, Germany). Spin labeling of tau was performed as described previously.<sup>8</sup>

**Aggregation Assay.** Monomeric htau40 (50 μM) was incubated with 12.5 μM heparin in 20 mM BES buffer, pH 7.4, and 1 mM DTT for 10 min at 95 °C to destroy the intramolecular disulfide bridges of compact monomers. After cooling down the reaction mixture to 37 °C, the sample was replenished with 1 mM DTT again, and a protease inhibitor mix (1 mM PMSF, 1 mM EDTA, 1 mM EGTA, 1 μg/mL leupeptin, 1 μg/mL aprotinin, and 1 μg/mL pepstatin) was added. The resulting solution was separated into different vials. PcTS was added to the vials in concentrations ranging from 200 pM to 200 μM, and the solutions were incubated for 10 days at 37 °C. DTT (1 mM) was added daily to avoid its depletion. Before each fluorescence measurement, the samples were equilibrated for 30 min at room temperature and diluted 6-fold with BES buffer followed by the addition of 20 μM ThS. Fluorescence was measured on a Safire (TECAN) fluorimeter with excitation and emission wavelengths of 440 and 521 nm, respectively. In addition, a 200 μM PcTS solution was prepared in the same buffer conditions to examine the absorption properties in the range 250–700 nm and to exclude possible interference with ThS fluorescence.

**Sodium Dodecyl Sulfate Polyacrylamide Gel Electrophoresis (SDS-PAGE) Analysis.** For SDS-PAGE analysis, 50 μM monomeric htau40 samples containing 1 mM DTT were prepared in 50 mM phosphate-buffered saline (PBS) buffer, pH 7.4, and heated for 20 min at 95 °C. After cooling down in a water bath, the samples were incubated with 750 μM PcTS for 1 or 24 h at 4 or 37 °C. Reference (Ferritin 440 kDa and protein marker) and control samples (htau40 in PBS buffer) were prepared, and all samples were run on 10% SDS-PAGE gels. Two additional htau40 samples were prepared in PBS and incubated for 3 days at 37 °C in the presence or absence of PcTS before running them on a 10% SDS-PAGE gel.

**Spin Labeling of Tau.** We constructed and labeled with (1-oxo-2,2,5,5-tetramethyl-D-pyrroline-3-methyl)-methanethiosulfonate (MTSL) the double cysteines of the wild-type (C291 and C322) as well as the mutants containing a single cysteine (C291A and C291A/C322G at different sites A15C, A72C, A125C, A178C, A239C, S352C, A384C, and S416C) using the following protocol: DTT was first removed from the buffer prior to labeling using size-exclusion chromatography (PD-10 columns, GE Healthcare, Freiburg, Germany); then, the monomeric protein was equilibrated in PBS buffer pH 7.4. MTSL (5-fold molar excess in ethyl acetate) was allowed to react with the free sulfhydryl group(s) of the cysteine(s) at 21 °C for 2.5 h. The unreacted spin label was removed by PD-10 columns

equilibrated in 50 mM Na phosphate buffer pH 6.8, and the resulting spin-labeled protein was concentrated by using Amicon Ultra-15 (molecular weight cutoff 3000, Millipore, Cork, Ireland).

**NMR Spectroscopy.** NMR experiments were recorded at 5 °C on Bruker Avance 700 or 800 MHz spectrometers equipped with cryogenic probes. NMR samples contained <sup>15</sup>N/<sup>13</sup>C double-labeled or <sup>15</sup>N single-labeled protein in 50 mM phosphate buffer pH 6.8, 1 mM DTT, and 10% (v/v) D<sub>2</sub>O. Different concentrations of PcTS were prepared in the same phosphate buffer, and the dilution factors were corrected whenever needed. For each measurement (except when time dependence was investigated), PcTS was freshly added to a sample of monomeric tau protein, and the measurement was started within less than 15 min. In the case of PcTS titrations, increasing concentrations of PcTS were subsequently added to the same tau sample with a delay of less than 10 min between individual heteronuclear single quantum coherence (HSQC) measurements. In order to probe the time dependence on NMR signal intensities, the samples were kept at room temperature for the specified time periods (3 and 7 days, Figure S3c, Supporting Information; 2 weeks, Figure S3d, Supporting Information).

Interaction of PcTS with 100 μM tau was investigated using two-dimensional (2D) <sup>1</sup>H–<sup>15</sup>N HSQC spectra recorded with 600 complex points and 32 scans per increment with spectral widths of 8389 and 1844 Hz in the <sup>1</sup>H and <sup>15</sup>N dimensions, respectively. The total measurement time for each <sup>1</sup>H–<sup>15</sup>N HSQC was 6 h. In the case of the control titration with 10 μM htau40 (Figure S6, Supporting Information), the recording time for a single <sup>1</sup>H–<sup>15</sup>N HSQC was increased to 20 h. NMR intensity ratio plots were reported with a 3-residues averaging window. 2D <sup>1</sup>H–<sup>13</sup>C HSQC spectra were acquired using 1024 complex points and 12 scans per increment with spectral widths of 7003 and 12 330 Hz (aliphatic region) or 5282 Hz (aromatic region) in the <sup>1</sup>H and <sup>13</sup>C dimensions, respectively, resulting in a total measurement time of 5 h. Spectra were processed with NMRPipe<sup>27</sup> and analyzed using the software Sparky3.

For equilibrium denaturation experiments, a solution of PcTS and <sup>15</sup>N-labeled htau40 (200 μM) in a ratio of 15:1 was prepared in 50 mM phosphate buffer pH 6.8, containing 1.8 mM DTT and 10% (v/v) D<sub>2</sub>O. A 2D <sup>1</sup>H–<sup>15</sup>N HSQC spectrum was measured for 3 h. Then, the denaturant concentration was increased, and at each denaturant concentration, a 2D <sup>1</sup>H–<sup>15</sup>N HSQC spectrum (measurement time: 3 h) was recorded. Denaturant solutions were prepared immediately before use, and concentrations ranged from 0 to 8 M for urea and from 0 to 3 M for GuSCN. NMR signal intensities were fitted to sigmoid, Hill, or exponential curve functions using Igor Pro 6.22A.

Paramagnetic relaxation enhancement (PRE) broadening was investigated using <sup>15</sup>N-labeled htau40 at a concentration of 15 μM. PRE effects were measured from the peak intensity ratios between two 2D <sup>1</sup>H–<sup>15</sup>N HSQC NMR spectra acquired in the presence of the nitroxide radical and after addition of 4 mM DTT (heated to 45 °C for 10 min before measurement) to the same sample. Addition of DTT will cleave the MTSL tag from the cysteine residue, such that the spin label is no longer attached to the protein and the protein is in the diamagnetic state. The measurement time for each 2D <sup>1</sup>H–<sup>15</sup>N HSQC NMR was 17 h.

NMR diffusion experiments were recorded on a Bruker Avance 600 MHz spectrometer equipped with cryogenic probe for htau40 protein (40 μM with or without 15-fold excess PcTS) using a stimulated-echo based pulsed gradient spin-echo sequence incorporating the WATERGATE solvent suppression.<sup>28</sup> The diffusion time and the length of the gradient pulses were optimized for each sample. The gradient strength was linearly increased from 2% to 95% of the maximum gradient strength in 30 steps, where the 100% gradient strength corresponds to 55.14 G/cm. Each <sup>1</sup>H spectrum was recorded with 128 scans and 16K complex over a spectral width of 8992 Hz, resulting in a total experimental time of 2 h for a complete NMR diffusion experiment. Several peaks in the aliphatic region of htau40 were selected, and the intensities of their diffusion-based spin-echo attenuation were extracted to determine an average diffusion coefficient. Note that the NMR-based characterization of the tau oligomers occurs via their flexible N- and C-terminal tails (Figure 2).

From the apparent diffusion coefficients of httau40 and a range of protein standards (cytochrome C 12.4 kDa, 17.8 Å; lysozyme 14.3 kDa, 20.5 Å; myoglobin 18 kDa, 21.2 Å; and ovalbumin 45 kDa, 30.5 Å), the Stokes radii were calculated.<sup>29</sup>

**EPR Spectroscopy.** Selected single-labeled httau40 (20 μM in phosphate buffer pH 6.8) samples were freshly prepared in the absence or presence of 15-fold excess PcTS and transferred in 1 mm inner diameter capillaries prior to each measurement. Continuous wave EPR spectra were recorded at room temperature at the X-band on a Bruker Elexys 500 spectrometer equipped with an ER 4122SHQE resonator. The incident power used was at 2.0 mW over a field range of 100 G and 1024 spectral points and a modulation amplitude of 0.8 G. The line broadening of the central peak of each spin-labeled httau40 was quantified using the width of the peak-to-peak separation. Integration of the EPR spectra in the absence and presence of PcTS resulted in similar double integral values, indicating that the same amount of tau protein contributes to the visible EPR signal in the absence and presence of PcTS.

**Fourier Transform Infrared (FTIR) Spectroscopy.** FTIR spectra of 50 μM K18 and 100 μM httau40 (with and without 1.5 mM PcTS) in 50 mM phosphate buffer were collected at room temperature using the Bruker Confocheck FTIR spectrometer. The delay time between preparation of the tau–PcTS sample and start of the FTIR measurements was about 10 min. The FTIR setup consists of the AquaSpec transmission cell designed for measurements of aqueous solutions and equipped with a cryogenic MCT detector cooled with liquid nitrogen. Reported spectra represent averages of 5 scans recorded between 3000 and 1000 cm<sup>-1</sup> where each scan was acquired with a spectral resolution of 4 cm<sup>-1</sup> and a measurement time of 100 s. The same measurement was repeated three times using freshly prepared samples to confirm the reproducibility of the results.

**Dynamic Light Scattering (DLS).** DLS measurements were performed at 5 °C using a DynaPro Titan temperature-controlled micro-sampler (Wyatt Technologies Corporation). Samples (40 μM httau40 in 50 mM phosphate buffer, pH 6.8, and 1 mM DTT inserted in 50 μL flow cells in absence or presence of 15-fold excess of PcTS) were illuminated by a 25 mW, 780 nm solid-state laser, and the intensity of 90° angle scattered light was measured at 4 μs intervals by a solid-state avalanche photodiode. Measurements were performed using freshly prepared samples; each experiment lasted 20 min and was repeated 6 times to confirm the reproducibility of the results (i.e., total of 2 h). The average values with their standard deviations were analyzed using the software package Dynamics 6.7.7.9.

**Circular Dichroism (CD).** CD spectra of 30 μM K18 and 10 μM httau40 in 50 mM phosphate buffer were acquired at room temperature using a Chirascan CD spectrometer (Applied Photophysics Limited) in the absence or presence of 15-fold excess of PcTS. Spectra were acquired with 350 μL in a cuvette with 1 mm path cell over the range covering 190–250 nm using a 1 nm bandwidth and a scanning speed of 20 nm/min. Five scans (measurement time for a single scan was 10 min) were averaged for each data set, and the subsequent spectra of the buffer constituents were subtracted from the protein samples. The same measurement was repeated at three times using freshly prepared samples to confirm the reproducibility of the results. Data are expressed in terms of the mean residual ellipticity ( $\theta$ , deg cm<sup>2</sup> dmol<sup>-1</sup>).

**Electron Microscopy.** The sample with the highest PcTS concentration (PcTS/httau40, 200 μM to 50 μM) from the aggregation assays was diluted 1:7.5 with 20 mM BES buffer, pH 7.4, and 5 μL was placed on copper 600<sub>mesh</sub> grids covered with carbon film. The sample was stained with 2% uranyl acetate after immunostaining with gold-labeled anti-tau antibody K9JA–gold<sub>10 nm</sub> and examined on a CM12 transmission electron microscope.

**Fluorescence-Activated Cell Sorting (FACS).** The assay was performed with inducible N2a cells expressing the four-repeat-domain construct with a single deletion at position 280 (K18ΔK280). Three wells contained 1 mL of cell suspension and 0.0005% Thioflavin S. Negative controls were not treated further. Positive controls were treated with 1 μg/mL doxycyclin. Samples were treated by addition of 50 μM PcTS and the same amount of doxycyclin. After incubation for 4 days at 37 °C, the floating and adherent cells were combined,

pelleted for 5 min (at 295g), and washed once with PBS buffer. Cells were counted in a BD FACS Canto TMII flow cytometry system. The cell distribution was determined by accessing the cell size from the forward scatter FSC and the cell granularity from the side scatter SSC. Cells with ThS-positive aggregates were measured by the fluorescent signal intensity in the FTIC channel ( $\lambda_{\text{excitation}} = 495 \text{ nm}$ ;  $\lambda_{\text{emission}} = 519 \text{ nm}$ ).

**SAXS Data.** Data were collected at X33 at the European Molecular Biology Laboratory on DORIS III (DESY) at a wavelength of 1.5 Å at 25 °C using a Pilatus 1 M photon counting detector. Samples were freshly prepared immediately prior to the SAXS measurements and contained tau concentrations from 2.5 to 10 mg/mL and 1.8 mM DTT in 50 mM phosphate buffer pH 6.8. At 15-fold excess of PcTS, data were measured before and after filtering using a centrifugal filter with a 0.2 μm cutoff (Millipore, Carrigtwohill, Ireland). Each sample was exposed to 8 frames of 15 s each, with consistency checks between frames. Data analysis was performed in ATSAS 2.3.<sup>30</sup> The average molecular masses of solutes were estimated from the intensity extrapolated to zero angle. The maximum diameter was estimated by indirect Fourier transform using ATSAS 2.3.<sup>30</sup> The amount of monomeric httau40 at intermediate PcTS concentrations was estimated using NMR spectroscopy (as described in the Supporting Information).

Estimation of the average number of tau molecules in soluble oligomers at intermediate PcTS/Tau ratios used a combination of NMR and SAXS. At 10-fold and 15-fold excesses of PcTS, residues G120–S400 were broadened beyond detection, demonstrating that tau has been completely converted into soluble oligomers. Thus, the SAXS signal for these samples can exclusively be attributed to tau oligomers. In contrast, at intermediate PcTS concentrations, both monomeric and oligomeric tau species were present (according to NMR and SDS-PAGE) complicating the SAXS analysis. Nevertheless, to allow a detailed analysis of the oligomeric tau species at these PcTS concentrations, we took advantage of NMR spectroscopy. By assuming that a similar region of tau is part of the oligomers formed at high and intermediate PcTS concentrations, an assumption that is supported by a comparison of the NMR broadening profiles at 5-fold and 15-fold excesses of PcTS (Figure 2a), the NMR signal intensity ratios of the residues in this region were averaged and used as an estimate for the amount of residual monomeric tau. The average oligomeric number  $n$  of the remaining fraction was then computed from the nominal concentration of tau, the percentage  $r$  of remaining monomer in solution (as estimated by NMR), and the absolute scattering intensity  $I(0)$  divided by the intensity for monomeric tau  $I_{\text{monomeric}}(0)$ :

$$n = \frac{\frac{I(0)}{I_{\text{monomeric}}(0)} - r}{1 - r} \quad (1)$$

Errors in the oligomeric number were estimated by taking the minimum and maximum of the following:

$$n(\text{el}(0), \text{er}) = \frac{\frac{I(0) \pm \text{el}(0)}{I_{\text{monomeric}}(0)} - r \mp \text{er}}{1 - r \mp \text{er}} \quad (2)$$

where  $\text{er}$  is the error for the monomer ratio (two times the standard deviation of relative NMR intensities in the region G120–S400) and  $\text{el}(0)$  is the error of the total scattering intensity, estimated to fall within one standard deviation of scattering intensities at different protein concentrations, respectively. Within the given range of values ( $I(0) \gg 1.0$  and  $1.0 > r \pm \text{er} > 0.02$ ), it is thus highly probable that  $n$  lies within the following limits:

$$\frac{\frac{I(0) + \text{el}(0)}{I_{\text{monomeric}}(0)} - r - \text{er}}{1 - r - \text{er}} \geq n \geq \frac{\frac{I(0) - \text{el}(0)}{I_{\text{monomeric}}(0)} - r + \text{er}}{1 - r + \text{er}} \quad (3)$$

## RESULTS

**PcTS Inhibits Tau Filament Formation.** The aggregation of tau protein in vitro is promoted by polyanions such as

heparin.<sup>31</sup> Using this approach, we tested the ability of PcTS (Figure 1a) to suppress fibrillization of htau40. Porphyrins do

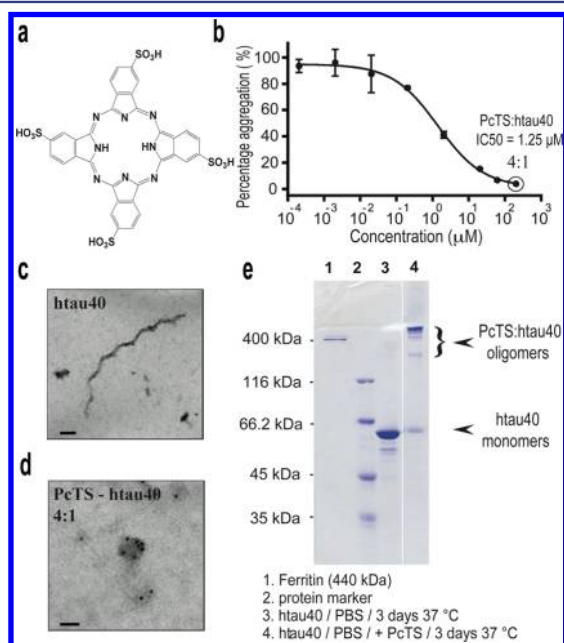


**Figure 1.** PcTS inhibits tau filament formation by induction of oligomers. (a) Chemical structure of PcTS. (b) ThS fluorescence after incubation of 50  $\mu\text{M}$  htau40 wild-type with 12.5  $\mu\text{M}$  heparin for 10 min at 95  $^{\circ}\text{C}$  and subsequent incubation for 10 days at 37  $^{\circ}\text{C}$  in the presence of increasing concentrations (200 pM to 200  $\mu\text{M}$ ) of PcTS. Electron micrographs of (c) heparin-induced htau40 aggregates showing PHF-like structures (scale bar, 100 nm) and (d) the sample treated with 4-fold molar excess of PcTS (scale bar, 40 nm). The black dots represent the gold-labeled antibody K9JA-gold<sub>10</sub> nm used for immunostaining. (e) SDS-PAGE analysis of PcTS-stimulated htau40 oligomers.

not interfere with the binding of tau to heparin excluding a competitive effect.<sup>16</sup> PcTS decreased the amount of fibrillized tau as quantified by thioflavin S (ThS) in a dose-dependent manner (Figure 1b). From the assay, we determined an IC<sub>50</sub> value of 1.25  $\mu\text{M}$ . For the 412 residue isoform htau34, an IC<sub>50</sub> value of 67  $\mu\text{M}$  was previously determined suggesting isoform-specific differences.<sup>16</sup> Using electron microscopy, we then investigated the morphology of htau40 that was incubated for 10 days at 37  $^{\circ}\text{C}$  in the absence and presence of a 4-fold molar excess of PcTS. In the absence of PcTS, we observed formation of tau filaments with the characteristic twisted appearance (Figure 1c). In contrast, globular particles and other amorphous aggregates were detected in the presence of PcTS (Figure 1d and Figure S2, Supporting Information). SDS-PAGE revealed predominantly two high molecular weight tau species with approximate molecular weights of 300 and 450 kDa (Figure 1e and Figure S3, Supporting Information). In addition, time-dependent changes in the distribution of high molecular weight species showed that the 450 kDa species becomes predominant with increasing incubation time (Figure S3a, Supporting Information).

#### Interaction with PcTS Is Mediated by Aromatic Rings.

To obtain insight into the mechanism of PcTS-induced oligomerization of tau, we probed the PcTS–tau interaction using NMR spectroscopy. Upon addition of PcTS, the intensities of several peaks in 2D  $^1\text{H}$ – $^{15}\text{N}$  HSQC spectra of htau40 decreased in a concentration-dependent manner

(Figure 2a). The broadening is caused by an exchange of tau molecules between the free and the PcTS-bound state. At

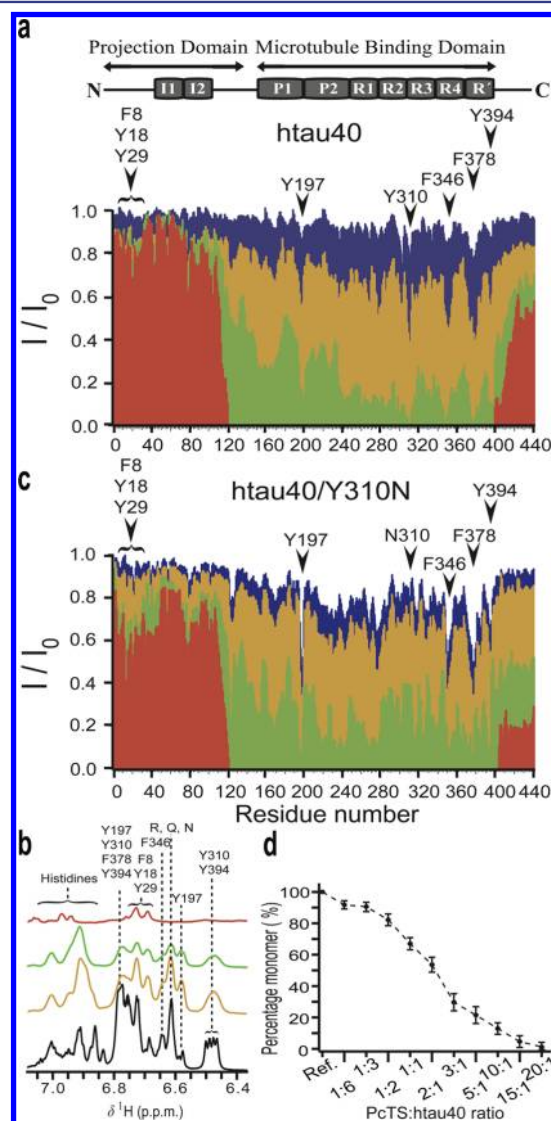


**Figure 2.** PcTS binds to aromatic rings of tau. (a) NMR signal broadening of 100  $\mu\text{M}$  htau40 at increasing PcTS concentrations (PcTS/Tau: 1:2, blue; 1:1, yellow; 5:1, green; 15:1, red) as a function of residue number. Aromatic residues of htau40 are marked. (b) One-dimensional  $^1\text{H}$  NMR spectra of htau40 in the absence (black) and presence of the corresponding ratios of PcTS. (c) NMR signal broadening of the htau40/Y310N variant at increasing PcTS concentrations. (d) Decrease of the concentration of monomeric tau at increasing PcTS concentrations. The residual monomer concentration was estimated from NMR broadening of the resonances of G120–S400 as shown in (a).

equimolar concentration of PcTS, the aromatic residues Y310, F346, and F378, which are located in the repeats R3–R4 and the C-terminal region, were most strongly affected (Figure 2a,b). In addition, Y197 in the proline-rich region P2 and Y394 bound to PcTS. Only weak changes in the NMR signal position and intensity were observed for the other three aromatic residues of htau40 (F8, Y18, and Y29) at the tau N terminus. The importance of aromatic residues was further supported by interaction studies performed for the tau mutant htau40/Y310N:  $^{306}\text{VQIVNK}^{311}$  showed reduced chemical shift and

intensity changes upon addition of PcTS (Figure 2c). Instead, stronger changes were observed for Y197, F346, and F378 indicative of an enhanced interaction. At 5:1 and 15:1 ratios of PcTS to htau40/Y310N, additional binding to the aromatic residues at the N terminus of tau occurred. We conclude that  $\pi$ - $\pi$  attractive forces between the PcTS aromatic ring and the aromatic residues of tau are responsible for the PcTS-tau interaction.

#### PcTS Stimulates Assembly of Soluble Tau Oligomers.

With increasing PcTS concentrations, we observed an overall decrease in NMR signal intensity for G120-S400 (Figure 2a,d). At 15-fold excess of PcTS, all signals in the central part of tau were broadened beyond detection indicating that residues in this region are too immobile to be detected by liquid-state NMR. This is in line with the PcTS-driven assembly of tau oligomers as evidenced by SDS-PAGE and electron microscopy (Figure 1d,e) and is supported by the disappearance of signals in  $^1\text{H}$ - $^{13}\text{C}$  HSQC spectra of htau24 and K18 (Figures S4 and S5, Supporting Information).

Importantly, highly similar NMR broadening profiles were observed at a 10-fold lower concentration of PcTS but keeping the same PcTS/Tau molar ratio (Figure S6, Supporting Information). As the self-stacking ability of PcTS is concentration dependent,<sup>32</sup> the data show that the signal broadening is not due to monomeric tau binding to large PcTS aggregates but because of stimulation of tau oligomer assembly by PcTS. Moreover, the NMR data reveal that not all regions in tau are immobilized in the tau oligomers, as residues M1-A119 and G401-L441 remained visible (Figure 2a).

**Remodeling of Tau Oligomers.** Biochemical analysis had revealed an increase in the concentration of SDS-resistant tau oligomers with increasing incubation time and temperature (Figure S3, Supporting Information). At the same time, NMR spectroscopy showed that PcTS rapidly converts tau from the monomeric state to oligomers; the total time from preparation of the tau-PcTS sample to completion of the 2D  $^1\text{H}$ - $^{15}\text{N}$  HSQC was 6 h (Figure 2a). Thus, PcTS rapidly stimulates formation of oligomers that are mostly not resistant to SDS but become more stable during incubation. In addition, time-dependent changes in the distribution of high molecular weight species—the ~450 kDa species becomes more pronounced—observed in SDS-PAGE point to a change in the structural properties of the PcTS-stimulated oligomers of tau with increasing incubation time (Figure S3a, Supporting Information). Consistent with the finding, we observed time-dependent changes in the NMR spectra of tau in the presence of 15-fold excess of PcTS. Two weeks after addition of PcTS, NMR signal intensities in the C-terminal tail of htau40 were decreased by an additional ~50% (Figure S3d, Supporting Information). The reduced signal intensities can be caused by a lower mobility of the tail, a stronger interaction with the core of the oligomer (see below), or the formation of an increased amount of oligomers, in which the C-terminal tail is rigidified and therefore not visible to NMR spectroscopy in solution.

**Tau Oligomers Have a Dynamic Core.** Paired helical filaments (PHFs) represent fibrous assemblies of tau with an amyloid-like core of rigid cross- $\beta$  structure.<sup>33</sup> The formation of cross- $\beta$  structure during *in vitro* heparin-induced aggregation of tau was observed by ThS in the absence of PcTS (Figure 1b). In the presence of PcTS, cross- $\beta$  structure was not formed, judging by the absence of the ThS signal (Figure 1b).

To obtain further insight into the secondary structure of PcTS oligomers, we performed CD and FTIR spectroscopic

measurements. The FTIR amide I ( $1655\text{ cm}^{-1}$ ) and II ( $1541\text{ cm}^{-1}$ ) bands are the vibrational bands that are most sensitive to protein secondary structure. However, no changes in their frequencies, and only minor changes in the other bands, were observed in the tau oligomers when compared to monomeric tau (Figure 3a). This is also supported by CD spectroscopy of

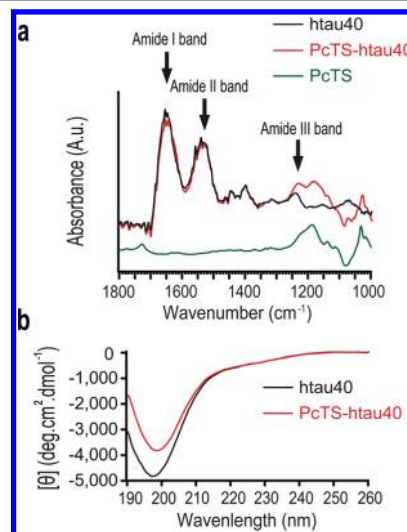


**Figure 3.** Secondary structure analysis of tau oligomers. (a) FTIR spectra of htau40 in the absence (black) and presence of a 15-fold excess of PcTS (red). (b) Far UV CD spectra of htau40 in the absence (black) and presence of a 15-fold excess of PcTS (red).

htau40 (Figure 3b) and the repeat domain construct K18 (Figure S7, Supporting Information). We conclude that tau oligomers stimulated by PcTS do not contain detectable elements of  $\alpha$  helix or  $\beta$  structure.

To obtain information about the dynamics within tau oligomers, we applied EPR spectroscopy to htau40 variants tagged with the paramagnetic nitroxide radical MTSL. In agreement with previous reports,<sup>34</sup> monomeric tau gave rise to EPR spectra with three sharp lines characteristic for a highly flexible protein backbone (Figure 4a). The EPR spectra of the PcTS-induced tau oligomer were more similar to that of monomeric tau with three clearly distinguishable lines. Indeed, for positions 15, 72, and 416, no difference with respect to monomeric tau was observed pointing to comparable mobility. However, for spin-label positions 125, 178, 239, 322, 352, and 384, EPR lines were broadened (Figure 4a,b), in particular, for sites 352 and 384 that are close to the aromatic residues F346, F378, and Y394 (Figures 2a and 4b). The line broadening is in line with the burial of these sites in the tau oligomer. At the same time, the EPR spectra of the tau oligomers are very different from those of PHFs, which had strongly reduced amplitude and lost the outer two hyperfine lines.<sup>34</sup> The EPR data thus demonstrate that the core of PcTS-stimulated tau oligomers remains dynamic.

**Global Folding within Tau Oligomers.** Next, we probed the long-range structure in the tau oligomers using PRE of NMR signals<sup>35</sup> (Figure 5). In addition, to the single cysteine mutants employed for EPR, we labeled the two native cysteines, C291 and C322, with MTSL. The paramagnetic nitroxide label results in broadening of amide resonances, which can be quantified through the NMR intensity ratios in the paramagnetic and diamagnetic states. The PRE effect scales as the inverse sixth power of the distance between the unpaired

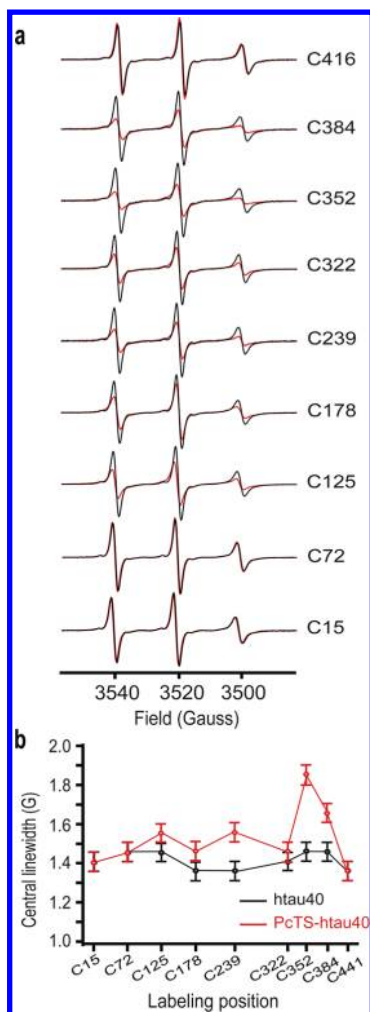


**Figure 4.** (a) EPR spectra of MTSL–cysteine-tagged htau40 at several positions in the absence (black, monomeric tau) and presence of PcTS (red, oligomeric tau). (b) Comparison of the EPR line width of the central line in the absence (black, monomeric tau) and presence of PcTS (red, oligomeric tau).

electron of the nitroxide unit and the NMR spin, providing a powerful probe of distances. Although residues in the microtubule-binding domain were too immobile to be detected, that is, are hidden in the oligomer, the flexible tails provided sensitive probes. When spin labels were attached to the native cysteines in wild-type tau, an approximately 10% decrease of the NMR broadening was observed at the N terminus when compared to monomeric tau (Figure 5d). On the other hand, a more pronounced broadening was induced at the C terminus with PRE intensity ratios of  $\sim 0.6$  (Figure 5d). The enhanced broadening at the C terminus demonstrates a transient interaction of the flexible tails with the NMR-invisible core of the tau oligomers. In contrast, little paramagnetic broadening was induced with a spin label at position 239 (Figure 5c). When compared to the network of transient long-range interactions in monomeric (Figure 5 and ref 8) and PHF tau,<sup>36</sup> the interaction of the N-terminal tail with the microtubule-binding domain is weakened, while that with the C terminus is tightened in PcTS-stimulated tau oligomers.

**PcTS-Stimulated Tau Oligomers Have a Compact Core.** At large excess of PcTS, tau is completely converted into soluble oligomers (Figure 2d). Pulsed-field gradient NMR

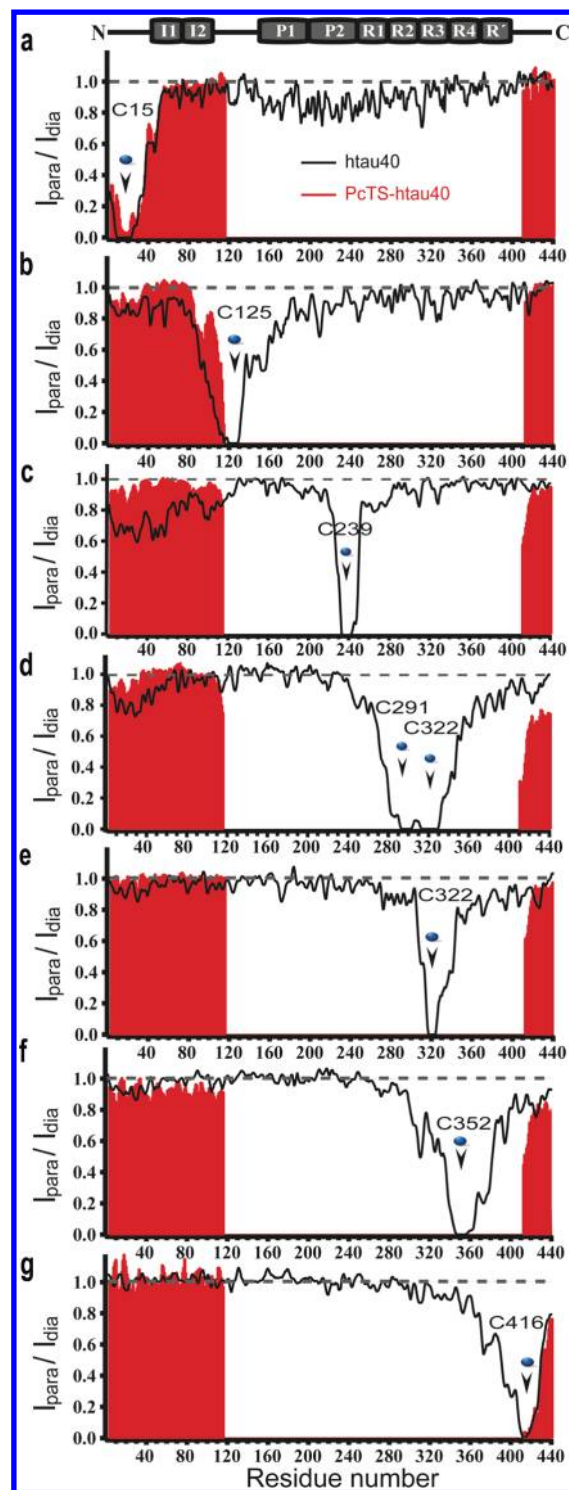


**Figure 5.** Changes in transient long-range interactions in tau upon incorporation into oligomers. PRE of backbone amide protons of MTSL spin-labeled htau40 at selected positions (a–g) in the absence (black) and presence of a 15-fold excess of PcTS (red). The plots show the intensity ratios between 2D  $^1\text{H}$ – $^{15}\text{N}$  HSQC spectra with the nitroxide in its paramagnetic and diamagnetic states.

and DLS showed an effective hydrodynamic radius of  $\sim 68$  Å (Figure 6). We then performed a SAXS analysis of tau at different protein and PcTS concentrations (Figure 7 and Figure S8, Supporting Information). The observed SAXS profile for monomeric tau is in line with its intrinsically disordered

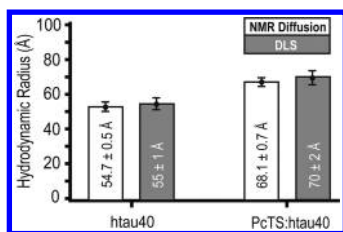


**Figure 6.** Hydrodynamic radius of monomeric and PcTS-stimulated oligomeric htau40 determined by pulsed-field gradient NMR and DLS.

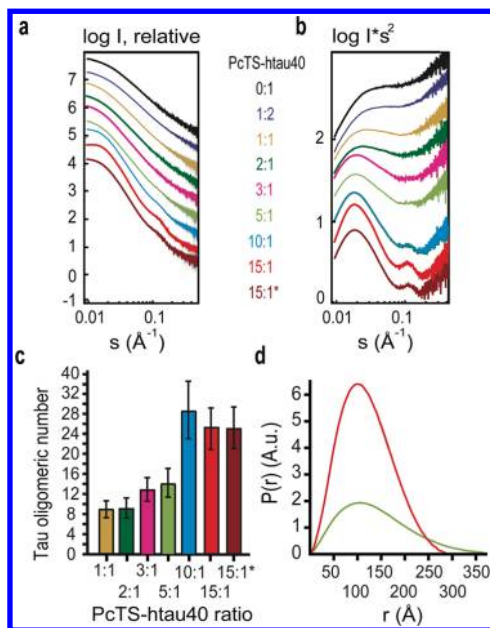


**Figure 7.** Low-resolution SAXS models of tau oligomers. (a) Experimental SAXS spectra and (b) Kratky plots of 10 mg/mL htau40 (black) alone and in the presence of increasing concentrations of PcTS (color coded panel). Note that the PcTS signal does not contribute significantly to the total scattering intensity (Figure S8, Supporting Information). (c) Estimation of the number of tau molecules in PcTS-stimulated oligomers at different PcTS/htau40 ratios (with htau40 at 2.5 mg/mL). The dark red bar shows the data for the 15:1 sample after filtering. Error bars were estimated from the standard error of  $I_0$  variations between different concentrations of htau40 but at the same ratio of PcTS and accounting for errors in the NMR-based estimation of the concentration of monomeric htau40 (see the Supporting Information). (d) The  $P(r)$  of tau oligomers at 5-fold (green) and 15-fold (red) excess of PcTS.

nature.<sup>37</sup> However, with increasing PcTS concentrations, the Kratky plot drastically changed (Figure 7b).

At 15-fold excess of PcTS, the Kratky plot revealed a sharp peak that is characteristic for the presence of highly compact tau species with an average radius of gyration of  $98 \pm 15$  Å. The average radius of gyration exceeds the hydrodynamic radius by a factor of  $\sim 1.4$  in line with the flexible disordered tails of the tau oligomers detected by NMR spectroscopy (Figure 2a). In addition to the changes in the Kratky plot, the scattering intensities strongly increased at higher PcTS/tau ratios.

Of note, PcTS alone scattered much weaker and therefore does not contribute substantially (Figure S8a, Supporting Information). The scattering intensities, corrected for the concentration of monomeric protein as determined by NMR spectroscopy (see the Experimental Section), showed that, already at an equimolar concentration, oligomeric species

containing approximately 5–11 tau molecules were formed and only slightly increased to 7–14 at 5-fold excess of PcTS (Figure 7c and Figures S7b,c, Supporting Information). In contrast, at the higher PcTS/Tau ratios of 10:1 and 15:1, the oligomeric species shifted to an average of  $\sim 24$  tau molecules. The maximum diameter,  $D_{\max}$  of the two oligomeric species was calculated as  $393 \pm 10$  and  $348 \pm 27$  Å, respectively (Figure 7d). The slightly smaller  $D_{\max}$  value at higher PcTS is supported by the sharpening of the peak in the Kratky plot (Figure 7b). Consistent with these observations, SDS-PAGE analysis revealed two predominant PcTS-induced tau species with approximate molecular weights of 300 and 450 kDa (Figure 1e).

**Tau Oligomers Are Stabilized Noncooperatively.** To obtain a detailed description of the conformational stability of different regions in the tau oligomers, we performed equilibrium denaturation experiments.<sup>38</sup> A comparison of NMR spectra obtained in 8 M urea and 3 M GuSCN revealed a distinct sensitivity of the tau oligomers to the two denaturants (Figure 8a–c and Figure S9, Supporting Information). All observable residues were classified into one of four groups depending on their urea denaturation profile (Figure 8d,e). The denaturation profiles differed between the groups, but within a group, residues displayed cooperative behavior (Figure 8e). Surprisingly, residues G120–T205 belonging to group III, which are broadened beyond detection in the tau oligomers, were very sensitive to low concentrations of urea. In contrast, residues in the second proline-rich region and the repeats were not detected even at 8 M urea demonstrating that they form the core of PcTS-stimulated oligomers of tau. The resistance to urea denaturation is in line with  $\pi$ – $\pi$  stacking as a key factor for oligomer stability.

Residues belonging to groups I and II from the urea denaturation roughly coincide with residues having a common denaturation profile in GuSCN (GuSCN group I) (Figure 8f,g). Strikingly, in the repeat region, signals were detected already at 0.1 mM GuSCN, demonstrating a very low stability of the tau oligomers in ionic denaturants. In addition, signal intensities in 3 M GuSCN were highly similar to those observed in monomeric tau (Figure S10, Supporting Information). The different denaturation profiles for individual residues indicate that the PcTS-stimulated tau oligomers are noncooperatively stabilized.

**PcTS Inhibits Tau Aggregation in Cells.** To investigate the impact of PcTS-induced oligomer formation on tau aggregation in cells, we used the neuroblastoma N2a cell model.<sup>39</sup> After 4 days of incubation at 37 °C, the fluorescence signal intensity of the ThS-positive aggregates was measured. The amount of ThS-positive cells in the untreated positive control was set to 100%. From this cell-based assay, we observe that PcTS leads to a 97% decrease in the fluorescence of ThS-positive cells relative to the untreated positive control (Figure 9), demonstrating that PcTS is a highly effective inhibitor of tau-induced aggregation in cells.

## DISCUSSION

Our study demonstrates that the organic compound phthalocyanine tetrasulfonate binds to specific aromatic residues of tau and inhibits tau filament formation by targeting tau into soluble oligomers. By using a combination of NMR spectroscopy, EPR spectroscopy, and SAXS, two predominant oligomeric species were revealed comprising  $\sim 7$ –14 and 24 tau molecules, respectively. The core of the soluble tau

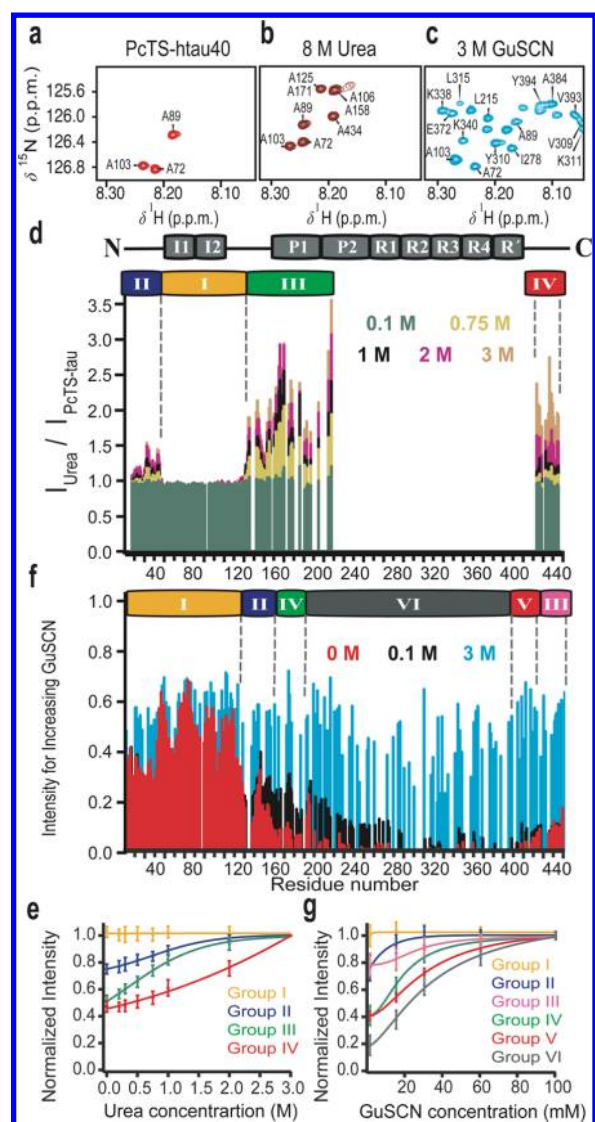


**Figure 8.** Stability of tau oligomers. (a) Selected region of 2D  $^1\text{H}$ - $^{15}\text{N}$  HSQC spectra of htau40 in the presence of a 15-fold excess of PcTS and after addition of (b) 8 M urea and (c) 3 M GuSCN. Resonances of residues that were rigidified in the tau oligomers (b) partially or (c) fully recovered. (d) Ratios of NMR signal intensities in 2D  $^1\text{H}$ - $^{15}\text{N}$  HSQC spectra of htau40 with 15-fold excess of PcTS at increasing urea concentrations ( $I_{\text{urea}}$ ) when compared to values in the absence of urea ( $I_{\text{PcTS-tau}}$ ). Increasing signal intensities indicate a residue-specific destabilization of the tau oligomers. (e) Urea denaturation profiles of PcTS-stimulated tau oligomers. All observable residues were classified into one of four groups based on their initial intensities, their sensitivity to urea concentration, and their intensities in 3 M urea. The denaturation profiles differed between the groups, but within a group, residues displayed cooperative behavior. (f) Residue-specific analysis of NMR signal intensities of PcTS/htau40 (15:1) at increasing concentrations of GuSCN. Only nonoverlapping peaks were included. Groups of residues (I–VI) that show a common profile of denaturation are marked above, and their denaturation profiles are shown in (g).

oligomers is highly compact with a maximum diameter of 30–40 nm (Figure 7) but is noncooperatively stabilized (Figure 8). Biochemical experiments and analyses in tau animal models suggested that tau oligomers and not PHFs might represent the acutely toxic species.<sup>9,40</sup> Tau oligomers prepared in vitro, which impair memory and cause synaptic dysfunction in mice,<sup>41</sup> were

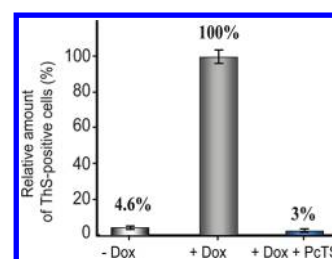


**Figure 9.** Percentage of ThS-positive cells determined by a FACS analysis of inducible N2a cells expressing the four-repeat domain proaggregation K18 $\Delta$ K280 construct. Cell suspensions containing either ThS alone (negative control) or ThS and doxycyclin without (positive control) or with 50  $\mu\text{M}$  PcTS (treated cell culture) were incubated for 4 days at 37  $^{\circ}\text{C}$ . The fluorescence signal intensity of ThS-positive aggregates was measured, and the amount of cells in the untreated positive control was set to 100%.

largely SDS-stable apparent trimers, displayed a spherical morphology, and contained  $\beta$ -sheet structure.<sup>42</sup> In contrast, tau oligomers stimulated by PcTS are only partially SDS-stable, are not spherical, and do not contain  $\beta$  structure (Figures 1–7), pointing to distinct structural properties of toxic tau oligomers.

Despite the highly compact core of PcTS-stimulated tau oligomers, significant heterogeneity is likely to remain both with respect to the species being present and the number of tau molecules in the oligomeric species. EPR spectroscopy demonstrated that even the compact core of tau oligomers remains highly dynamic (Figure 4). The dynamic nature of the oligomer is in clear contrast to the pronounced rigidity of the  $\beta$ -sheet rich core of tau amyloid fibrils.<sup>34</sup> In addition, the EPR line broadening observed for the spin labels at positions 352 and 384 (Figure 4), in comparison to spin-label positions in the C-terminal domain, suggest that this region is more rigid or compact in tau oligomers. This region also contains the three aromatic residues F346, F378, and Y394 that comprise the primary binding sites for PcTS (Figure 2a). In contrast, the  $\beta$ -sheet rich core of PHFs is located more to the N-terminal part of the repeat region extending at most to residue  $\sim$ 355.<sup>43–45</sup> Thus, the location of the compact core of PcTS-stimulated tau oligomers and tau filaments is partially distinct in line with the finding that PcTS-stimulated tau oligomers cannot convert into tau filaments.

## CONCLUSION

PcTS belongs to the family of cyclic tetrapyrroles, is planar with a hydrophobic central aromatic macrocyclic structure, and carries four negatively charged sulfonate groups at its peripheral outer benzo substitution positions. Previously, it was shown that PcTS binds to the aromatic residues of  $\alpha$ -synuclein in the monomeric protein.<sup>22,46,47</sup> Here, we demonstrate that PcTS inhibits formation of tau filaments in vitro and in cells (Figures 1 and 9) by selectively interacting with residues Y197, Y310, F346, F378, and Y394 in the central domain of tau and converting into soluble oligomers. The specific interaction with aromatic residues in the central domain of tau, and not with aromatic residues at the N terminus, is distinct from a nonselective sequestration of protein molecules due to self-association of anti-amyloid agents.<sup>48</sup> It is also distinct from the nonselective mechanism that involves the covalent linkage via lysine residues into high molecular weight oligomers as suggested for the polyphenol oleocanthal.<sup>19,49</sup>

Site-directed mutagenesis indicated that the different PcTS-binding sites in tau are independent (Figure 2c). In addition, the observation that soluble tau oligomers are formed in the absence of a single residue, Y310, supports a key role of PcTS-stimulated oligomer formation for the inhibition of tau aggregation. While Y310 is buried in the fibrillar core of PHFs,<sup>36,43</sup> Y197 and Y394 remain accessible for interaction with PcTS providing a mechanism for the previously demonstrated dissolution of tau filaments by PcTS.<sup>16</sup>

In summary, we revealed detailed insights into the mechanism of tau aggregation inhibition and the structure and dynamics of soluble tau oligomers. Our study indicates that the structure of off-pathway oligomers of tau is distinct from the structure of toxic tau oligomers.

## ■ ASSOCIATED CONTENT

### ● Supporting Information

Overview over tau isoforms; changes in chemical shifts of tau induced by PcTS; time-dependent changes in NMR intensity profiles; interaction of PcTS with the tau fragment K18 and tau isoform htau24; influence of PcTS concentration on NMR broadening; FTIR and CD spectra of K18 in absence and presence of PcTS; SAXS of PcTS-stimulated tau oligomers; 2D <sup>1</sup>H–<sup>15</sup>N HSQC spectra and signal intensities. This material is available free of charge via the Internet at <http://pubs.acs.org>.

## ■ AUTHOR INFORMATION

### Corresponding Author

Markus.Zweckstetter@dzne.de; Eckhard.Mandelkow@dzne.de

### Author Contributions

#These authors contributed equally to this work.

### Notes

The authors declare no competing financial interest.

## ■ ACKNOWLEDGMENTS

We thank Marina Bennati and Eva-Maria Mandelkow for stimulating discussion and Ilka Lindner for sample preparation. This work was funded through the Cluster of Excellence and DFG Research Center “Nanoscale Microscopy and Molecular Physiology of the Brain”, the MPG consortium Toxic Protein Conformation, the Metlife Foundation, the Tau Consortium, and the DFG (ZW 71/3-2 to M.Z.).

## ■ REFERENCES

- (1) Ross, C. A.; Poirier, M. A. *Nat. Med.* **2004**, *10* (Suppl), S10.
- (2) Forman, M. S.; Lee, V. M.; Trojanowski, J. Q. *J. Chem. Neuroanat.* **2000**, *20*, 225.
- (3) Hardy, J.; Selkoe, D. J. *Science* **2002**, *297*, 353.
- (4) Goedert, M.; Spillantini, M. G. *Science* **2006**, *314*, 777.
- (5) Cleveland, D. W.; Hwo, S. Y.; Kirschner, M. W. *J. Mol. Biol.* **1977**, *116*, 227.
- (6) Schweers, O.; Schonbrunn-Hanebeck, E.; Marx, A.; Mandelkow, E. *J. Biol. Chem.* **1994**, *269*, 24290.
- (7) Drubin, D.; Kirschner, M. *J. Cell Biol.* **1986**, *103*, 2739.
- (8) Mukrasch, M. D.; Bibow, S.; Korukottu, J.; Jeganathan, S.; Biernat, J.; Griesinger, C.; Mandelkow, E.; Zweckstetter, M. *PLoS Biol.* **2009**, *7*, e34.
- (9) Lasagna-Reeves, C. A.; Castillo-Carranza, D. L.; Jackson, G. R.; Kaye, R. *Curr. Alzheimer Res.* **2011**, *8*, 659.
- (10) Pul, R.; Dodel, R.; Stangel, M. *Expert Opin. Biol. Ther.* **2011**, *11*, 343.
- (11) Noble, W.; Planel, E.; Zehr, C.; Olm, V.; Meyerson, J.; Suleman, F.; Gaynor, K.; Wang, L.; LaFrancois, J.; Feinstein, B.; Burns, M.;

Krishnamurthy, P.; Wen, Y.; Bhat, R.; Lewis, J.; Dickson, D.; Duff, K. *Proc. Natl. Acad. Sci. U.S.A.* **2005**, *102*, 6990.

(12) Zhang, B.; Maiti, A.; Shively, S.; Lakhani, F.; McDonald-Jones, G.; Bruce, J.; Lee, E. B.; Xie, S. X.; Joyce, S.; Li, C.; Toleikis, P. M.; Lee, V. M.; Trojanowski, J. Q. *Proc. Natl. Acad. Sci. U.S.A.* **2005**, *102*, 227.

(13) Wischik, C. M.; Edwards, P. C.; Lai, R. Y.; Roth, M.; Harrington, C. R. *Proc. Natl. Acad. Sci. U.S.A.* **1996**, *93*, 11213.

(14) Pickhardt, M.; von Bergen, M.; Gazova, Z.; Hascher, A.; Biernat, J.; Mandelkow, E. M.; Mandelkow, E. *Curr. Alzheimer Res.* **2005**, *2*, 219.

(15) Crowe, A.; Ballatore, C.; Hyde, E.; Trojanowski, J. Q.; Lee, V. M. *Biochem. Biophys. Res. Commun.* **2007**, *358*, 1.

(16) Taniguchi, S.; Suzuki, N.; Masuda, M.; Hisanaga, S.; Iwatsubo, T.; Goedert, M.; Hasegawa, M. *J. Biol. Chem.* **2005**, *280*, 7614.

(17) Bulic, B.; Pickhardt, M.; Schmidt, B.; Mandelkow, E. M.; Waldmann, H.; Mandelkow, E. *Angew. Chem., Int. Ed.* **2009**, *48*, 1740.

(18) Chirita, C.; Necula, M.; Kuret, J. *Biochemistry* **2004**, *43*, 2879.

(19) Li, W.; Sperry, J. B.; Crowe, A.; Trojanowski, J. Q.; Smith, A. B., III; Lee, V. M. *J. Neurochem.* **2009**, *110*, 1339.

(20) Ehrnhoefer, D. E.; Bieschke, J.; Boeddrich, A.; Herbst, M.; Masino, L.; Lurz, R.; Engemann, S.; Pastore, A.; Wanker, E. E. *Nat. Struct. Mol. Biol.* **2008**, *15*, 558.

(21) Woods, L. A.; Platt, G. W.; Hellewell, A. L.; Hewitt, E. W.; Homans, S. W.; Ashcroft, A. E.; Radford, S. E. *Nat. Chem. Biol.* **2011**, *7*, 730.

(22) Lamberto, G. R.; Binolfi, A.; Orcelet, M. L.; Bertoncini, C. W.; Zweckstetter, M.; Griesinger, C.; Fernandez, C. O. *Proc. Natl. Acad. Sci. U.S.A.* **2009**, *106*, 21057.

(23) Caughey, W. S.; Raymond, L. D.; Horiuchi, M.; Caughey, B. *Proc. Natl. Acad. Sci. U.S.A.* **1998**, *95*, 12117.

(24) Priola, S. A.; Raines, A.; Caughey, W. S. *Science* **2000**, *287*, 1503.

(25) Park, J. W.; Ahn, J. S.; Lee, J. H.; Bhak, G.; Jung, S.; Paik, S. R. *ChemBioChem* **2008**, *9*, 2602.

(26) Mukrasch, M. D.; Biernat, J.; von Bergen, M.; Griesinger, C.; Mandelkow, E.; Zweckstetter, M. *J. Biol. Chem.* **2005**, *280*, 24978.

(27) Delaglio, F.; Grzesiek, S.; Vuister, G. W.; Zhu, G.; Pfeifer, J.; Bax, A. *J. Biomol. NMR* **1995**, *6*, 277.

(28) Zheng, G.; Stait-Gardner, T.; Anil Kumar, P. G.; Torres, A. M.; Price, W. S. *J. Magn. Reson.* **2008**, *191*, 159.

(29) Jones, J. A.; Wilkins, D. K.; Smith, L. J.; Dobson, C. M. *J. Biomol. NMR* **1997**, *10*, 199.

(30) Konarev, P. V.; Petoukhov, M. V.; Volkov, V. V.; Svergun, D. I. *J. Appl. Crystallogr.* **2006**, *39*, 277.

(31) Goedert, M.; Jakes, R.; Spillantini, M. G.; Hasegawa, M.; Smith, M. J.; Crowther, R. A. *Nature* **1996**, *383*, 550.

(32) Boyle, R. W.; Dolphin, D. *Photochem. Photobiol.* **1996**, *64*, 469.

(33) Berriman, J.; Serpell, L. C.; Oberg, K. A.; Fink, A. L.; Goedert, M.; Crowther, R. A. *Proc. Natl. Acad. Sci. U.S.A.* **2003**, *100*, 9034.

(34) Margittai, M.; Langen, R. *Proc. Natl. Acad. Sci. U.S.A.* **2004**, *101*, 10278.

(35) Gillespie, J. R.; Shortle, D. *J. Mol. Biol.* **1997**, *268*, 170.

(36) Bibow, S.; Mukrasch, M. D.; Chinnathambi, S.; Biernat, J.; Griesinger, C.; Mandelkow, E.; Zweckstetter, M. *Angew. Chem., Int. Ed.* **2011**, *50*, 11520.

(37) Mylonas, E.; Hascher, A.; Bernado, P.; Blackledge, M.; Mandelkow, E.; Svergun, D. I. *Biochemistry* **2008**, *47*, 10345.

(38) Schulman, B. A.; Kim, P. S.; Dobson, C. M.; Redfield, C. *Nat. Struct. Biol.* **1997**, *4*, 630.

(39) Pickhardt, M.; Biernat, J.; Khlistunova, I.; Wang, Y. P.; Gazova, Z.; Mandelkow, E. M.; Mandelkow, E. *Curr. Alzheimer Res.* **2007**, *4*, 397.

(40) Brunden, K. R.; Trojanowski, J. Q.; Lee, V. M. *J. Alzheimer's Dis.* **2008**, *14*, 393.

(41) Lasagna-Reeves, C. A.; Castillo-Carranza, D. L.; Sengupta, U.; Clos, A. L.; Jackson, G. R.; Kaye, R. *Mol. Neurodegener.* **2011**, *6*, 39.

(42) Lasagna-Reeves, C. A.; Castillo-Carranza, D. L.; Guerrero-Muoz, M. J.; Jackson, G. R.; Kaye, R. *Biochemistry* **2010**, *49*, 10039.

(43) Andronesi, O. C.; von Bergen, M.; Biernat, J.; Seidel, K.; Griesinger, C.; Mandelkow, E.; Baldus, M. *J. Am. Chem. Soc.* **2008**, *130*, 5922.

(44) Daebel, V.; Chinnathambi, S.; Biernat, J.; Schwalbe, M.; Habenstein, B.; Loquet, A.; Akoury, E.; Tepper, K.; Muller, H.; Baldus, M.; Griesinger, C.; Zweckstetter, M.; Mandelkow, E.; Vijayan, V.; Lange, A. *J. Am. Chem. Soc.* **2012**, *134*, 13982.

(45) von Bergen, M.; Barghorn, S.; Muller, S. A.; Pickhardt, M.; Biernat, J.; Mandelkow, E. M.; Davies, P.; Aebi, U.; Mandelkow, E. *Biochemistry* **2006**, *45*, 6446.

(46) Rao, J. N.; Dua, V.; Ulmer, T. S. *Biochemistry* **2008**, *47*, 4651.

(47) Lamberto, G. R.; Torres-Monserrat, V.; Bertocini, C. W.; Salvatella, X.; Zweckstetter, M.; Griesinger, C.; Fernandez, C. O. *J. Biol. Chem.* **2011**, *286*, 32036.

(48) McGovern, S. L.; Caselli, E.; Grigorieff, N.; Shoichet, B. K. *J. Med. Chem.* **2002**, *45*, 1712.

(49) Monti, M. C.; Margarucci, L.; Tosco, A.; Riccio, R.; Casapullo, A. *Food Funct.* **2011**, *2*, 423.